Complex Valued State Space Model for Weakly Nonlinear Duffing Oscillator with Noncollocated External Disturbance

Han Woong Yoo * **Georg Schitter** *

* *Automation and Control Institute (ACIN), TU Wien, Gusshausstr. 27-29, 1040 Vienna, Austria (e-mail: {yoo, schitter}@acin.tuwien.ac.at).*

Abstract: This paper proposes a slow flow model for a weakly nonlinear and parametrically driven Duffing oscillator and a complex valued state space model for the oscillator with noncollocated external disturbances. The combination of the parametrically driven duffing oscillator and noncollocated disturbances can be observed in resonant MEMS mirrors with a reinforcement structure to reduce dynamic mirror deformation. The model is based on a rational function approximation for the angular derivative of the out-of-plane comb drive capacitance, enabling qualitative analysis at large amplitudes while the stability analysis is maintained as the conventional cubic function approximation. The slow flow model is extended including a single tone noncollocated disturbance and is linearized at an equilibrium point for a small disturbance. The linearized disturbance model is reformulated by a complex valued state space model to cope with general wideband disturbances, allowing various analytic methods in traditional system theory. The simulation results demonstrate a good agreement between the proposed models and the ODE simulation, verifying the accuracy and benefits of the proposed models.

Keywords: Duffing oscillator, complex valued model, perturbation theory, disturbance model, noncollocated disturbance, MEMS mirror, automotive lidar

1. INTRODUCTION

For MEMS mirrors designed for various scanning applications such as pico projectors (Hsu et al. (2008)) and lidars (Hofmann et al. (2013); Brunner et al. (2019)), a well-known figure of merit is $\theta_{max} \cdot D \cdot f$ product, i.e. a multiplication of the maximum deflection angle, the size of the mirror, and the scanning frequency (Holmström et al. (2014)). The reason behind is that the number of pixels are defined by the maximum deflection angle, optical resolution depends on the mirror size, and the frequency defines the line or frame rate of the scanning system, and high number of this figure of merit allows high resolution and high definition imaging. To achieve a large angle, large aperture, and fast oscillation at the same time is, however, difficult due to design tradeoffs.

One of the main limiting factors in the MEMS mirror design is dynamic mirror deformation (Urey et al. (2000)), causing a blurred and degraded light spot in its size and shape. The analysis simply shows that more mirror thickness is required to maintain the dynamic deformation for a larger mirror, which increases the inertia significantly. Several approaches has been studied to reduce this additional burden on the inertia (Farrugia et al. (2018)). One idea uses a reinforcement structure with a thin mirror to reduce the low order surface deformation with a modest inertia increase (Nee et al. (2000); Milanovic et al. (2004);

Hsu et al. (2008)). Hofmann et al. (2013) shows a finite element analysis to evaluate dynamic deformation with various choices on reinforcement structure. However, a thick reinforcement structure may result in a mismatch between the rotational axis and the center of mass of the mirror, which can make the MEMS mirror susceptible to external vibrations (Yoo et al. (submitted)). This is crucial for some applications such as automotive lidars (Wolter et al. (2005)). Currently no analysis has been made so far on this disturbance influence for resonant MEMS mirrors with a reinforcement structure.

The contributions of this paper are the developments of the slow flow model based on an approximation of the torque and its linearized state space model for a parametrically driven Duffing oscillator with noncollocated disturbances. The noncollocated disturbances with the parametric oscillator are observed in resonant MEMS mirrors with a reinforcement structure in hash environment conditions, e.g. automotive MEMS lidars. For an analysis at large amplitudes, a rational function is used as an approximation for the angular derivative of an out-of-plane comb drive capacitance, keeping the stability properties as the conventional cubic function approximation (Lee (2007); Linzon et al. (2013); Ataman and Urey (2006)). The slow flow model is extended for an additional single tone noncollocated disturbance, which is due to the mismatch between the center of mass and the rotational axis of the mirror. By its linearization, a complex valued state space model is derived for general wideband disturbances, enabling various analytic tools in system theory. Numerical sim-
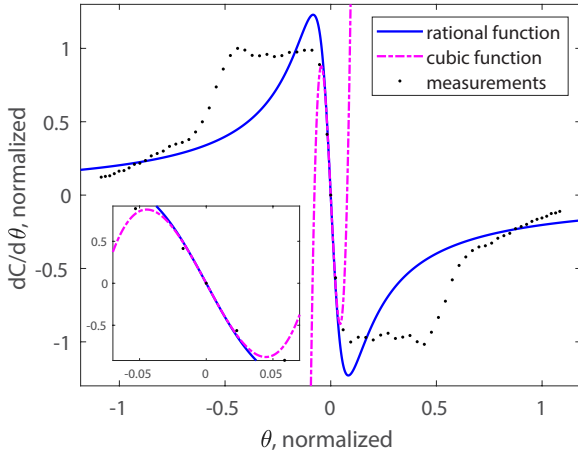
Fig. 1. Rational function (blue solid line) and cubic function approximation (magenta dashed dot line) for the measured angular derivative of an out-of-plane comb drive capacitance (black dots).

ulation results verify the accuracy and the computational efficiency of the developed models.

2. PROBLEM DESCRIPTION

Consider a Duffing oscillator with a positive cubic spring constant k_3 as

$$I\ddot{\theta} + c\dot{\theta} + k_1\theta + k_3\theta^3 = \frac{1}{2}\frac{dC}{d\theta}V^2 + \tau_{dy}, \qquad (1)$$

where θ is the mechanical deflection angle of the mirror, I denotes the inertia of the mirror, c is the linear damping parameter, and k_1 denotes the linear spring constant. The comb drive torque is defined by a product of the squared input voltage of V and the angular derivative of the comb drive capacitance of C. For convenience in analysis, the input voltage is set by a square rooted sine, i.e. $V^2(t) = U^2\left(\frac{1+\cos\Omega t}{2}\right)$, where U is the peak input voltage and Ω denotes the actuation frequency. τ_{dy} is an additional torque caused by a disturbance.

2.1 Comb drive torque model based on a rational function

The angular derivative of the comb drive capacitance is modeled by a rational function as (Lee (2007); Linzon et al. (2013))

$$\frac{dC}{d\theta} = \frac{\alpha\theta}{\theta^2 + \theta_0^2}, \qquad (2)$$

where α and θ_0 are the actuator model parameters. This rational function approximation has several benefits. First, the rational function has a steep gradient near the zero angle defined by a ratio of α to θ_0^2, which keeps stability analysis at the zero amplitude as cubic function approximation (Ataman and Urey (2006)). Secondly, the extreme points can be located at a low angle and the value approaches to zeros without a sign change as the mechanical angle increases. Finally, it is an analytic function for all θ, allowing various analytic tools such as perturbation theory.

Fig. 1 illustrates a rational function approximation and a cubic function approximation of the measured angular derivative of a comb drive capacitance, which is of a variant MEMS mirror on one in (Brunner et al. (2019)). The
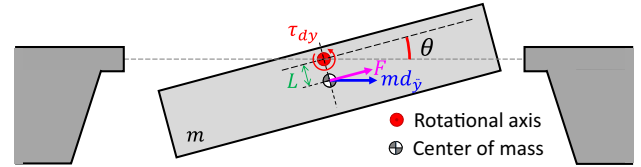

Fig. 2. Noncollocated disturbance model of an oscillating MEMS mirror. Due to the mismatch between the rotational axis and the center of mass, the disturbance $d_{\ddot{y}}$ along y axis changed into the disturbance induced torque τ_{dy} to the MEMS mirror.

rational function approximation still has mismatches from the measurements while it preserves the exact gradient near the zero angle and the overall trend at large angles. This allows qualitatively analysis on the MEMS mirror in a wide deflection angle.

2.2 Noncollocated disturbance model

Assume an acceleration $d_{\ddot{y}}$ along y axis as an external disturbance to the oscillating mirror. Noncollocated disturbances occur when the external acceleration is applied to the center of mass of the mirror while the mirror rotates at a distinct rotational axis. Fig. 2 shows an example of the noncollocated disturbance in case of unbalanced mirror thickness along the mirror rotational axis. The disturbance induced torque on the rotational axis is given by (Yoo et al. (submitted))

$$\tau_{dy} = mLd_{\ddot{y}}\cos\theta, \qquad (3)$$

where m and L denote the mass of the mirror and the length between the rotational axis and the center of mass, respectively. The disturbance torque is scaled by the cosine of the mirror angle due to the movement of the center of mass. The acceleration on the z axis also influences in a similar way. Further discussions can be found in (Yoo et al. (submitted)).

3. ANALYTIC MODELS OF THE OSCILLATOR WITH DISTURBANCES

The parametrically driven Duffing oscillator with its disturbance provides understanding how the external vibration influences to the oscillator. Due to the nonlinearity and inhomogeneity, however, the exact analytic solution is barely available while the brute-force numerical simulation of (1) requires a large computational effort. Perturbation theory with dimensionless formulation allows a good approximation of the solution (Nayfeh (1981)). This section derives a slow flow model from (1), (2), and (3) by the averaging method, and attain a complex valued state space model for general wideband disturbances by the linearization at the stationary solutions.

3.1 Duffing oscillator with a rational function torque model

First of all, a dimensionless form of the dynamic equation is derived by the normalized angle as $x(\tau) = \theta/\theta_0$ with the normalized time $\tau = t/t_0$ where $t_0 = \sqrt{I/k_1}$, and the normalized actuation frequency $\Omega_a = \Omega t_0$. Then Eq. (1) and (2) can be rewritten as

$$\ddot{x} + 2\mu\dot{x} + x + K_3x^3 = \frac{\alpha_n x}{x^2 + 1}\left(1 + \cos\Omega_a\tau\right), \qquad (4)$$

where the normalized damping, cubic stiffness, and actuator model parameters are defined by

$$\mu = \frac{ct_0}{2I}, \quad K_3 = \frac{k_3\theta_0^2 t_0^2}{I}, \quad \alpha_n = \frac{\alpha t_0^2 U^2}{4I\theta_0^2}, \tag{5}$$

respectively. From (Nayfeh (1981); Han et al. (2018)), Eq. (4) can be rewritten as

$$\ddot{x} + \sigma^2 x = \epsilon \left[-2\mu\dot{x} + \left(\sigma^2 - 1\right)x - K_3 x^3 \right.$$
$$\left. + \frac{\alpha_n x}{x^2 + 1}\left(1 + \cos\Omega_a\tau\right) \right], \tag{6}$$

where ϵ is a book keeping parameter for small perturbation and separates high order terms from the approximation. σ denotes an oscillation frequency, which is defined by a half of the actuation frequency, i.e. $\sigma = \Omega_a/2$. The normalized time τ can be rewritten as $T_i = \epsilon^i\tau$, i.e. $T_0 = \tau$, $T_1 = \epsilon\tau$. Assume that nonlinearities in the right hand side of (6) is small so that solution can be approximated by $x = x_0 + \epsilon x_1$. With partial derivative operators defined as $D_i = \frac{\partial}{\partial T_i}$ and by considering only the terms of ϵ^0 and ϵ^1, Eq. (6) can be rewritten as

$$D_0^2 x_0 + \sigma^2 x_0 = 0, \tag{7}$$
$$D_0^2 x_1 + \sigma^2 x_1 = \Psi(x_0, \sigma, T_0) - 2D_0 D_1 x_0, \tag{8}$$

where

$$\Psi(x_0, \sigma, T_0) = -2\mu D_0 x_0 + \left(\sigma^2 - 1\right)x_0 - K_3 x_0^3 + \frac{\alpha_n x_0}{x_0^2 + 1}$$
$$\times \left(1 + \cos 2\sigma T_0\right). \tag{9}$$

From (7), the approximated solution is given by

$$x_0 = A(T_1)\cos\left(\sigma T_0 + \beta(T_1)\right), \tag{10}$$

where $A(T_1)$ and $\beta(T_1)$ denote the amplitude and the phase of the mirror in the slow evolution along T_1, respectively. The solvability condition by averaging along a period (Nayfeh (1981); Elshurafa et al. (2011)) provides

$$\int_0^{2\pi} \left(\Psi(x_0, \sigma, T_0) - 2D_0 D_1 x_0\right)e^{-i\omega}d\omega = 0, \tag{11}$$

where ω is an integration variable, defined by $\omega = \sigma T_0 + \beta(T_1)$. For $A \geq 0$, the real part and the imaginary part of (11) generate partial differential equations of the phase and the amplitude of the oscillator, respectively. For $A > 0$, this leads to a slow flow model as

$$\frac{\partial A}{\partial T_1} = -\mu A - \frac{\alpha_n(2 + A^2 - 2\sqrt{1 + A^2})}{\sigma A^3}\sin 2\beta, \tag{12}$$

$$\frac{\partial \beta}{\partial T_1} = \frac{3K_3 A^2}{8\sigma} - \frac{(\sigma^2 - 1)}{2\sigma} - \frac{\alpha_n\left(1 - \frac{1}{\sqrt{1+A^2}}\right)}{A^2\sigma}$$
$$- \frac{\alpha_n(2 + A^2 - 2\sqrt{1 + A^2})}{\sigma A^4\sqrt{1 + A^2}}\cos 2\beta. \tag{13}$$

The name "slow flow" is defined by the different time scale compared to the original dynamics of (4). Primary frequencies can be obtained by the solution of stationary points, i.e. $\frac{\partial A}{\partial T_1} = 0$, $\frac{\partial \beta}{\partial T_1} = 0$, as

$$\sigma^2 = 1 + \frac{3K_3 A^2}{4} - \frac{2\alpha_n\left(1 - \frac{1}{\sqrt{1+A^2}}\right)}{A^2} \pm \frac{2\sigma}{\sqrt{1 + A^2}}$$
$$\times \sqrt{\left(\frac{\alpha_n(2 + A^2 - 2\sqrt{1 + A^2})}{A^4\sigma}\right)^2 - \mu^2}. \tag{14}$$

Eq. (14) cannot be fully solved analytically, but the solution can be obtained by an iterative manner with an initial unit frequency, i.e. $\sigma \approx 1$. The phase solution satisfies both (12) and (13) to resolve ambiguity of the inverse sine and cosine. By applying $\alpha_n = 0$ to (13), the well known backbone curve of the Duffing oscillator is obtained as well.

3.2 Duffing oscillator with a noncollocated disturbance

The slow flow model of (12) and (13) is extended with the additional noncollocated disturbance. As a simple case, a single tone sinusoidal signal is considered, i.e.

$$d_{\ddot{y}} = a_y \cos(\Omega_{yd}t + \phi_y), \tag{15}$$

where a_y denotes the acceleration amplitude along the y axis with its frequency of Ω_{yd} and phase of ϕ_y. This single tone disturbance allows an analysis by the averaging method in perturbation theory and is used in various studies for nonlinear oscillators with more than two external forces (Nayfeh (1981); Yagasaki et al. (1990)).

With the dimensionless parameters in Sec. 3.1, the disturbance frequency $\Omega_{yd} = \Omega_y t_0$ is added. Since the nonlinear cosine term in the disturbance is also approximated by Taylor series for a small angle of θ, the dimensionless dynamics of (1) and (3) is given as

$$\ddot{x} + 2\mu\dot{x} + x + K_3 x^3 = \frac{\alpha_n x}{x^2 + 1}\left(1 + \cos\Omega_a\tau\right) + mLa_y$$
$$\times \left(d_{y0} - d_{y2}x^2\right)\cos(\Omega_y\tau + \phi_y), \tag{16}$$

where normalized disturbance parameters are defined by

$$d_{y0} = \frac{t_0^2}{I\theta_0}, \quad d_{y2} = \frac{t_0^2\theta_0}{2I}. \tag{17}$$

The slow flow model is derived by the similar procedure as Sec. 3.1. By the solvability condition in (11), the averaged terms of the disturbance are obtained by the real part as

$$\frac{1}{2\pi\sigma A}\int_0^{2\pi}\frac{1}{4}\left\{(4d_{y0} - 3d_{y2}A^2)\cos\omega - d_{y2}A^2\cos 3\omega\right\}$$
$$\times mLa_y\cos(\Omega_y\tau + \phi_y)d\omega, \tag{18}$$

and by the imaginary part as

$$\frac{1}{2\pi\sigma}\int_0^{2\pi}\frac{1}{4}\left\{(4d_{y0} - d_{y2}A^2)\sin\omega - d_{y2}A^2\sin 3\omega\right\}$$
$$\times mLa_y\cos(\Omega_y\tau + \phi_y)d\omega. \tag{19}$$

Due to the approximated $\cos\theta$, the integrals of (18) and (19) result in the frequency difference between the disturbance frequency and the mirror frequency and between the disturbance frequency and the 3rd harmonic frequency. The high order odd harmonics can be coupled if the high order Taylor approximation is required for significantly large amplitudes. Without loss of generality, the disturbance frequencies near the mirror frequency are considered as

$$\Omega_y T_0 = \sigma T_0 + \delta_y T_1, \quad \delta_y = \frac{\Omega_y - \sigma}{\epsilon} \tag{20}$$

where δ_y denotes the frequency difference between the mirror frequency and the disturbance frequency. Substitute (20) into (18) and (19), the slow flow model of (12) and (13) is extended as

$$\frac{\partial A}{\partial T_1} = -\mu A - \frac{a_n(2 + A^2 - 2\sqrt{1 + A^2})}{\sigma A^3}\sin 2\beta$$
$$- d_{yA}(A, \sigma)mLa_y \sin(\beta - \delta_y T_1 - \phi_y), \quad (21)$$

$$\frac{\partial \beta}{\partial T_1} = \frac{3K_3 A^2}{8\sigma} - \frac{(\sigma^2 - 1)}{2\sigma} - \frac{a_n\left(1 - \frac{1}{\sqrt{1+A^2}}\right)}{A^2\sigma}$$
$$- \frac{a_n(2 + A^2 - 2\sqrt{1 + A^2})}{\sigma A^4 \sqrt{1 + A^2}}\cos 2\beta$$
$$- d_{y\beta}(A, \sigma)mLa_y \cos(\beta - \delta_y T_1 - \phi_y), \quad (22)$$

where the disturbance coefficients are defined by

$$d_{yA}(A, \sigma) = \frac{1}{8\sigma}(4d_{y0} - d_{y2}A^2), \quad (23)$$

$$d_{y\beta}(A, \sigma) = \frac{1}{8\sigma}(4d_{y0}A^{-1} - 3d_{y2}A). \quad (24)$$

This slow flow model approximates the behavior of the Duffing oscillator with a single tone noncollocated disturbance. These sine and cosine terms with a frequency δ_y lead to an invariant tori (Yagasaki et al. (1990)). In addition, the sine term in (21) is influenced by the sign of the frequency difference δ_y, which results in a distinct response for negative frequency differences compared to that for positive frequency differences. Before illustrating the distinct frequency response for negative frequency differences, the slow flow model is further investigated by linearization.

3.3 Linearization of the slow flow model

For further analysis on the invariant tori, the local dynamics of the Duffing oscillator is approximated by a linearized model at a stationary solution. At the specific frequency of $\bar{\sigma}$, the amplitude and the phase near the i-th stationary amplitude solution and phase solution, $\bar{A}_i$ and $\bar{\beta}_i$, respectively, are assumed by (Yagasaki et al. (1990))

$$A_i(T_1) = \bar{A}_i(\bar{\sigma}) + \varepsilon\xi(\bar{A}_i, \bar{\beta}_i, \bar{\sigma}, T_1),$$
$$\beta_i(T_1) = \bar{\beta}_i(\bar{\sigma}) + \varepsilon\zeta(\bar{A}_i, \bar{\beta}_i, \bar{\sigma}, T_1),$$

where ξ and ζ denote the linearized amplitude and phase error of the oscillator, respectively. ε is the other book keeping parameter that is multiplied to the disturbances to define it as a small signal and is used for Taylor approximations of the nonlinear terms to eliminate the high order terms from the approximation. The linearization of (21) and (22) results in a model as

$$\dot{\mathbf{x}}_{\mathbf{r}} = \mathbf{A_s}\mathbf{x_r} + \mathbf{B_{yr}}\mathbf{u_{yr}}, \quad (25)$$

where the state vector $\mathbf{x_r} \in \mathbb{R}^2$, the disturbance input vector $\mathbf{u_{yr}} \in \mathbb{R}^2$, the system matrix $\mathbf{A_s} \in \mathbb{R}^{2\times 2}$, and the disturbance input matrix $\mathbf{B_{yr}} \in \mathbb{R}^{2\times 2}$ are defined by

$$\mathbf{x_r} = \begin{bmatrix} \xi \\ \zeta \end{bmatrix}, \mathbf{u_{yr}} = \begin{bmatrix} a_y \cos(\delta_y T_1 + \phi_y) \\ a_y \sin(\delta_y T_1 + \phi_y) \end{bmatrix},$$

$$\mathbf{A_s} = \begin{bmatrix} A_{11} & A_{12} \\ A_{21} & A_{22} \end{bmatrix}, \mathbf{B_{yr}} = \begin{bmatrix} B_{11,y} & B_{12,y} \\ B_{21,y} & B_{22,y} \end{bmatrix},$$

respectively. The elements of $\mathbf{A_s}$ are given by

$$A_{11} = -\mu + \frac{\alpha_n A_{11,s}\sin 2\bar{\beta}_i}{\bar{\sigma}\bar{A}_i^4\sqrt{1 + \bar{A}_i^2}},$$

$$A_{12} = -\frac{2\alpha_n(2 + \bar{A}_i^2 - 2\sqrt{1 + \bar{A}_i^2})\cos 2\bar{\beta}_i}{\bar{\sigma}\bar{A}_i^3},$$
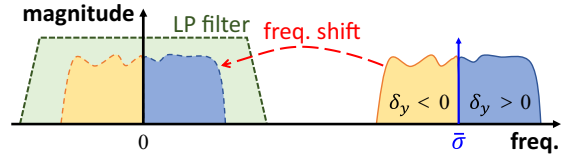

Fig. 3. Procedure of an image reject down converter for generating the complex disturbance variable. The banded signal around the mirror frequency $\bar{\sigma}$ is shifted to the zero frequency and a low pass filter is applied to remove unnecessary high frequency components.

$$A_{21} = \frac{3K_3\bar{A}_i}{4\bar{\sigma}} - \frac{\alpha_n\left(2 + 3\bar{A}_i^2 - 2(1 + \bar{A}_i^2)^{\frac{3}{2}}\right)}{\bar{\sigma}\bar{A}_i^3(1 + \bar{A}_i^2)^{\frac{3}{2}}} - \frac{\alpha_n A_{21,c}\cos 2\bar{\beta}_i}{\bar{\sigma}\bar{A}_i^5\left(1 + \bar{A}_i^2\right)^{\frac{3}{2}}},$$

$$A_{22} = \frac{2\alpha_n(2 + \bar{A}_i^2 - 2\sqrt{1 + \bar{A}_i^2})\sin 2\bar{\beta}_i}{\bar{\sigma}\bar{A}_i^4\sqrt{1 + \bar{A}_i^2}},$$

$$A_{11,s} = \bar{A}_i^2\left(-4 + \sqrt{1 + \bar{A}_i^2}\right) + 6\left(-1 + \sqrt{1 + \bar{A}_i^2}\right),$$

$$A_{21,c} = -3\bar{A}_i^4 + 8\left(-1 + \sqrt{1 + \bar{A}_i^2}\right) + 4\bar{A}_i^2\left(-3 + 2\sqrt{1 + \bar{A}_i^2}\right),$$

and the elements of $\mathbf{B_{yr}}$ are

$$B_{11,y} = -d_{yA}(\bar{A}_i, \bar{\sigma})mL\sin\bar{\beta}_i, \; B_{12,y} = d_{yA}(\bar{A}_i, \bar{\sigma})mL\cos\bar{\beta}_i,$$
$$B_{21,y} = -d_{y\beta}(\bar{A}_i, \bar{\sigma})mL\cos\bar{\beta}_i, \; B_{22,y} = -d_{y\beta}(\bar{A}_i, \bar{\sigma})mL\sin\bar{\beta}_i.$$

The linearized model of (25) provides a fast solution of oscillator dynamics with a disturbance. However, the generation of $\mathbf{u_{yr}}$ needs both sine and cosine terms, which hampers further analysis on general wideband disturbances.

3.4 Complex valued state space model for general wideband disturbances

Since Eq. (25) considers a local linear model for a small disturbance, superposition of various frequency components can generalize the disturbance. This leads to a complex valued state space model as

$$\dot{\mathbf{x}} = \mathbf{A_s}\mathbf{x} + \mathbf{B_y}\mathbf{u_y}, \quad (26)$$

where $\mathbf{x}$ denotes the complex valued state vector, i.e. $\mathbf{x} \in \mathbb{C}^2$. The complex disturbance input matrix $\mathbf{B_y} \in \mathbb{C}^{2\times 1}$ and the complex disturbance variable $\mathbf{u_y} \in \mathbb{C}$ are given by

$$\mathbf{B_y} = \begin{bmatrix} B_{11,y} - jB_{12,y} \\ B_{21,y} - jB_{22,y} \end{bmatrix}, \mathbf{u_y} = \int_{-\infty}^{\infty} a_y(\delta_y)e^{\phi_y(\delta_y)}e^{j\delta_y T_1}d\delta_y,$$
$$(27)$$

where a_y and ϕ_y are extended as a function of δ_y. The complex disturbance input variable is just an inverse Fourier transform, and it is generally complex valued signal since the frequency components at positive and negative frequency differences are usually not conjugated. Assuming full-state measurements, the influence of the disturbance $\mathbf{y}$ is the real part of the state variable, i.e. $\mathbf{y} = \text{Re}(\mathbf{x})$ and $\mathbf{y} \in \mathbb{R}^2$.

Besides, the disturbance $d_{\ddot{y}}$ to the oscillator for (15) and (20) can be generalized by

$$d_{\ddot{y}} = \int_{-\infty}^{\infty} a_y(\delta_y)e^{\phi_y(\delta_y)}e^{j\left(\delta_y + \frac{\bar{\sigma}}{\epsilon}\right)T_1}d\delta_y. \quad (28)$$

Since $d_{\ddot{y}}$ is a real signal, the coefficients satisfies $a_y(\delta_y) = a_y(-2\bar{\sigma}/\epsilon - \delta_y)$ and $\phi_y(\delta_y) = -\phi_y(-2\bar{\sigma}/\epsilon - \delta_y)$. If the generalized disturbance is bandlimited, $d_{\ddot{y}}$ can be converted

to the complex disturbance variable $\mathbf{u_y}$ by an image reject down converter (Martin (2004)) as

$$\mathbf{u_y} = (d_{\ddot{y}} \times e^{-j\bar{\sigma}\tau}) * p_L(\tau), \qquad (29)$$

where $p_L(\tau)$ denotes the impulse response of the low pass filter and $*$ is a convolution operator. Fig. 3 shows the procedure of an image reject down converter. First, the frequency components near $\bar{\sigma}$ are shifted to near zero. This procedure also shifts the frequency components near $-\bar{\sigma}$ to near $-2\bar{\sigma}$. To remove these high frequency components, the low pass filter of p_L is applied, which leads to $\mathbf{u_y}$. In general, the disturbance violates this bandlimit assumption, causing aliasing, but the influence can be still approximated by a bandlimited signal since the system of (26) is bandlimited.

The complex valued state space model can be converted to a complex valued transfer function as

$$\begin{bmatrix} \Xi(s) \\ Z(s) \end{bmatrix} = (\mathbf{A_s}(\bar{A}_i, \bar{\beta}_i, \bar{\sigma}) - s\mathbf{I})^{-1}\mathbf{B_y}(\bar{A}_i, \bar{\beta}_i, \bar{\sigma}), \qquad (30)$$

where $\Xi(s)$ and $Z(s)$ are the disturbance transfer functions of the amplitude error and the phase error of the oscillator. These complex valued models allow various analytic tools and methods in system theory (Troeng et al. (2017)), enabling control and observer design with the consideration of the disturbance. A simple analysis example is discussed in the following section.

4. SIMULATION VERIFICATION

This section provides numerical verification of the proposed models for a parametrically driven Duffing oscillator with a noncollocated disturbance. First, the slow flow model is verified by the primary frequencies, a set of stationary solutions. Next, the proposed complex valued models are analyzed using a pole zero map and frequency responses for single tone disturbances. Finally, the models are evaluated with a general wideband disturbance. For verification, the ODE simulator in (Brunner et al. (2019)) is used as a reference since it describes the full nonlinear behavior of (1) and allows any disturbance. The amplitude and phase of the ODE simulation results are sampled by every period of the input voltage for comparison.

4.1 Primary frequency of the nonlinear slow flow model

Fig. 4 illustrates primary frequencies by the slow flow model in (14) along the various amplitudes, compared to the ODE simulation results of (1). The stability of the solutions is determined by $\mathbf{A_s}$ of (25), and the stable solutions and unstable solutions are drawn with solid lines and dotted lines, respectively. For most amplitudes, the analytic solution of (14) matches well with the numerical solutions of (1). As shown in Fig. 4(a), the resonance peak by the ODE simulation is only 1.4 % larger amplitude and 0.2 % higher frequency than that of the slow flow model, proving the accuracy of the proposed slow flow model. Comparing to the measured mirror response curve in (Brunner et al. (2019)), the qualitative behavior of the models is similar including bifurcations. This also verifies that the rational function approximation is also a reasonable choice for the model of an out-of-plane comb drive to analyze behaviors at large amplitudes.
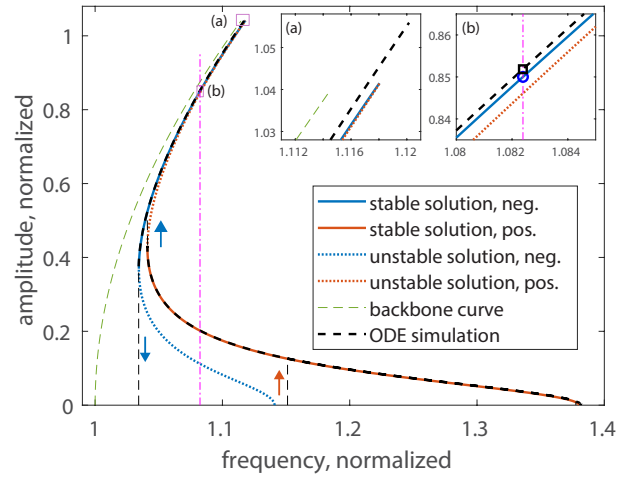

Fig. 4. Primary frequencies by the slow flow model (blue and red solid and dotted line) and the numerically obtained stationary solutions (thick black dashed lines) and bifurcations (thin black dashed lines) by the ODE simulation. The backbone curve (green dashed line) by the slow flow model is drawn as a reference.
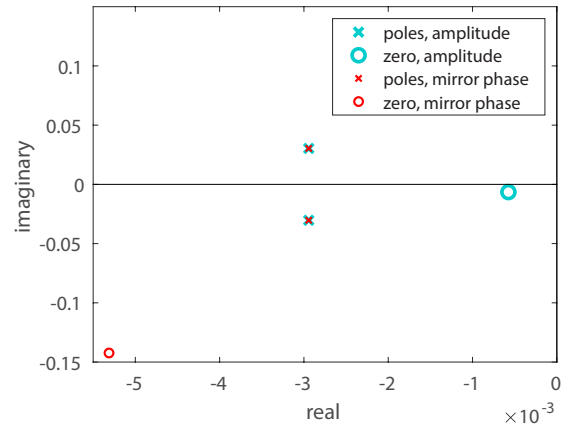

Fig. 5. Pole zero map of the amplitude and mirror phase transfer function.

4.2 Frequency response of single tone disturbances

The complex valued model of (30) contains complex conjugate poles with an arbitrary complex zero since $\mathbf{B_y}$ is the only complex valued matrix. For the disturbance analysis, an amplitude of 0.85 is chosen as an operational point, which is marked by a blue circle in Fig. 4(b). Fig. 5 illustrates the pole zero map for the complex valued transfer function of amplitude and phase errors. In both cases, the poles are complex conjugated while the zero is a single complex value in negative frequencies.

Fig. 6 illustrates the frequency response of the complex valued transfer functions for positive and negative frequency differences of δ_y. Due to the location of the complex zeros in Fig. 5, the complex zeros influence only negative δ_y, resulting in a deep notch and smaller resonance peaks compared to that of the positive δ_y. The frequency response is verified by the transient responses of single tone disturbances with the slow flow model of (21) and (22) and the ODE simulation of (1), (3), and (15). For the ODE simulation, the operational point has a slight
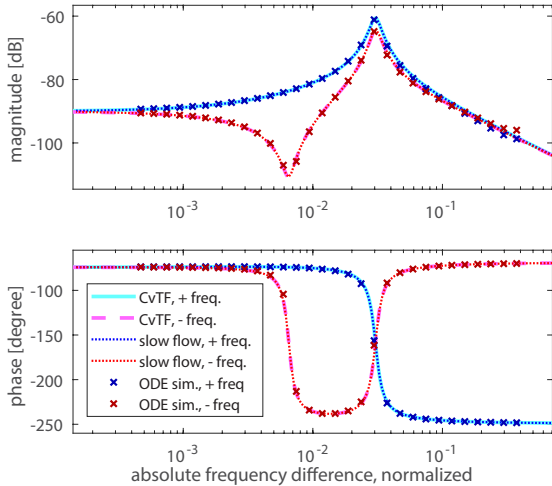
(a) amplitude error ξ
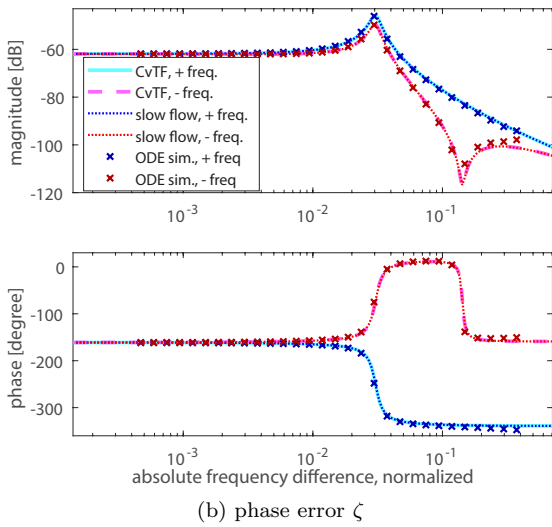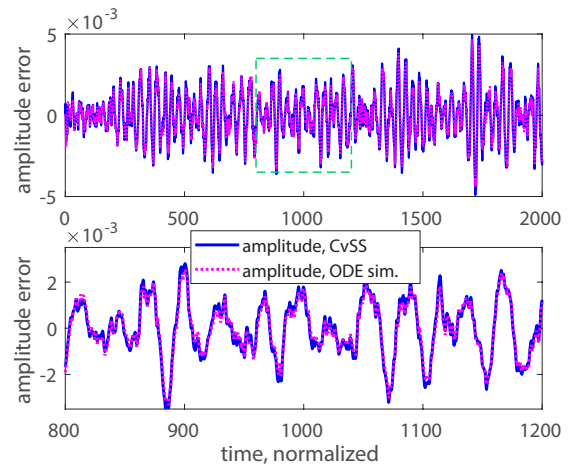

(b) phase error ζ

Fig. 6. Frequency responses of the complex valued transfer function (CvTF) of the Duffing oscillator with the noncollocated disturbance along the absolute frequency differences $|\delta_y|$ (light blue colored solid line for positive δ_y and light red dashed line for negative δ_y), which are compared to the single tone disturbance influences using the slow flow model (dark dotted lines) and the ODE simulation (x marks).

higher amplitude (a black square) at the same frequency $\bar{\sigma}$ (magenta dashed dot line) in Fig. 4(b), which is due to the approximation error of the slow flow model. While the responses of the ODE simulation slightly increase at high frequency differences due to aliasing, the complex valued transfer function show a good agreement with both the slow flow model and the ODE simulation. This verifies the accuracy of the proposed complex valued models for single tone disturbances.

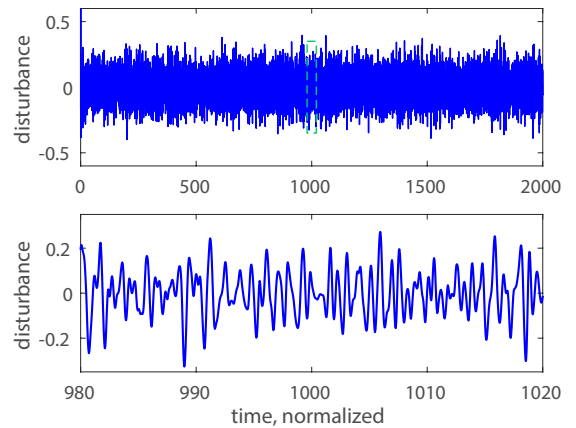### 4.3 Transient response for general wideband disturbances

The complex valued state space model is evaluated for a general wideband disturbance to analyze the influences in time domain. The general wideband disturbance is generated by a Gaussian random noise, filtered by a zero phase bandpass filter with a passband of $\bar{\sigma} \pm 0.706$ in normalized frequency. In the generation of the complex

(a) amplitude error ξ and zoomed plot (green square)
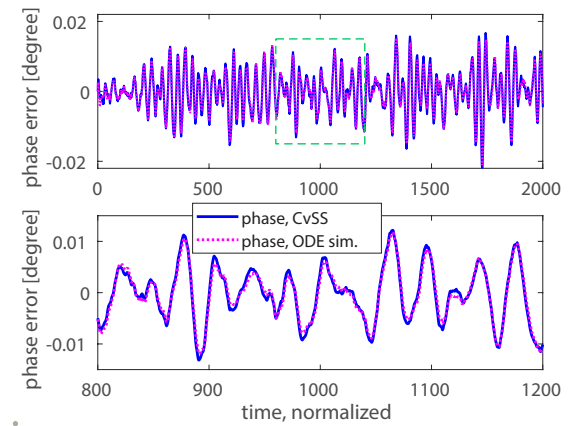
(b) phase error ζ and zoomed plot (green square)

(c) generalized disturbance d_{ij} and zoomed plot (green square)

Fig. 7. Transient responses of amplitude and phase errors by the complex valued state space model (CvSS) and the ODE simulation by a general wideband disturbance.

disturbance variable, a zero phase lowpass filter is used as an extension of (29) to remove the phase lag during the image reject down conversion. For comparison, the ODE simulation evaluates the response with the general wideband disturbance. For the ODE simulation, the start point of the disturbance is matched with a zero phase of the mirror actuation for simplicity.

Fig. 7 shows transient responses of the amplitude error and phase error by the disturbance using the complex valued state space model and the ODE simulation. The overall response of the complex valued model shows a good match with the ODE simulation. The normalized mean square errors (NMSE) for the amplitude error trajectory between two models are 0.0289 and that of phase error trajectory is 0.0307. For the simulation time, the ODE simulation takes 403.08 s while the complex valued model only takes 0.64 s by a laptop PC (Matlab 2018b, Intel Core-i7 8850H, 2.6 GHz). Although the level of information are different, the proposed model shows high computational efficiency compared to the brute force simulation.

These results prove that the proposed complex valued models for noncollocated disturbances provides an accurate and computationally efficient solution, allowing a fast and systematic analysis on disturbances for resonant MEMS mirrors with a reinforcement structure.

5. CONCLUSION

The influences of noncollocated disturbances are analyzed for a weakly nonlinear and parametrically driven Duffing oscillator based on perturbation theory and the complex valued state space model. First of all, a rational function approximates the angular derivative of an out-of-plane comb drive capacitance, allowing a qualitative analysis at large amplitudes. Then a slow flow model is derived with the rational function approximation and is extended by the noncollocated disturbances, leading to a complex valued state space model. The numerical verification of the primary frequencies illustrates the accuracy of the proposed slow flow model compared to the ODE simulation. The frequency responses of single tone disturbances show that the proposed complex valued model matches well with the results of the slow flow model and the ODE simulation. The transient response by a general wideband disturbance shows also a good agreement with the ODE simulation, showing normalized mean square errors of 0.0289 and 0.0307 in amplitude and phase errors, respectively. The computation time by the proposed complex valued model is significantly shorter than the ODE simulation. This verifies the proposed complex valued models for resonant MEMS mirrors with noncollocated disturbances, enabling further systematic analysis and control system design for a robust operation in applications under harsh vibrations e.g. automotive lidars.

ACKNOWLEDGEMENTS

REFERENCES

Ataman, C. and Urey, H. (2006). Modeling and characterization of comb-actuated resonant microscanners. *J. Micromech. Microeng.*, 16(1), 9.

Brunner, D., Yoo, H.W., Thurner, T., and Schitter, G. (2019). Data based modelling and identification of nonlinear SDOF MOEMS mirror. In *Proc. SPIE 10931*, 1093117.

Elshurafa, A.M., Khirallah, K., Tawfik, H.H., Emira, A., Aziz, A.K.S.A., and Sedky, S.M. (2011). Nonlinear dynamics of spring softening and hardening in folded-MEMS comb drive resonators. *J. Microelectromech. Syst.*, 20(4), 943–958.

Farrugia, R., Grech, I., Camilleri, D., Casha, O., Gatt, E., and Micallef, J. (2018). Theoretical and finite element analysis of dynamic deformation in resonating micromirrors. *Microsyst Technol*, 24(1), 445–455.

Han, J., Li, L., Jin, G., Feng, J., Li, B., Jia, H., and Ma, W. (2018). Vibration Identification of Folded-MEMS Comb Drive Resonators. *Micromachines*, 9(8), 381.

Hofmann, U., Aikio, M., Janes, J., Senger, F., Stenchly, V., Hagge, J., Quenzer, H.J., Weiss, M., Wantoch, T.v., Mallas, C., Wagner, B., and Benecke, W. (2013). Resonant biaxial 7-mm MEMS mirror for omnidirectional scanning. *J. Micro/Nanolith. MEMS MOEMS*, 13(1), 011103.

Holmström, S.T.S., Baran, U., and Urey, H. (2014). MEMS laser scanners: A review. *J. Microelectromech. Syst.*, 23(2), 259–275.

Hsu, S., Klose, T., Drabe, C., and Schenk, H. (2008). Fabrication and characterization of a dynamically flat high resolution micro-scanner. *J. Opt. A: Pure Appl. Opt.*, 10(4), 044005.

Lee, K.B. (2007). Non-contact electrostatic microactuator using slit structures: theory and a preliminary test. *J. Micromech. Microeng.*, 17(11), 2186–2196.

Linzon, Y., Ilic, B., Lulinsky, S., and Krylov, S. (2013). Efficient parametric excitation of silicon-on-insulator microcantilever beams by fringing electrostatic fields. *J. of Appl. Phys.*, 113(16), 163508.

Martin, K. (2004). Complex signal processing is not complex. *IEEE Trans. Circuits Syst. I, Reg. Papers*, 51(9), 1823–1836.

Milanovic, V., Matus, G., and McCormick, D. (2004). Gimbal-less monolithic silicon actuators for tip-tilt-piston micromirror applications. *IEEE J. Sel. Topics Quantum Electron.*, 10(3), 462–471.

Nayfeh, A.H. (1981). *Introduction to perturbation techniques*. Wiley, New York.

Nee, J., Conant, R., Muller, R., and Lau, K. (2000). Lightweight, optically flat micromirrors for fast beam steering. In *2000 IEEE/LEOS Int. Conf. on Opt. MEMS*, 9–10.

Troeng, O., Bernhardsson, B., and Rivetta, C. (2017). Complex-coefficient systems in control. In *Proc. Am. Control Conf.*, 1721–1727. IEEE, Seattle, WA, USA.

Urey, H., Wine, D.W., and Osborn, T.D. (2000). Optical performance requirements for MEMS-scanner-based microdisplays. In *Proc. SPIE vol. 4178*, 176–185.

Wolter, A., Hsu, S.T., Schenk, H., and Lakner, H.K. (2005). Applications and requirements for MEMS scanner mirrors. In *Proc. SPIE 5719*, 64–76.

Yagasaki, K., Sakata, M., and Kimura, K. (1990). Dynamics of a weakly nonlinear system subjected to combined parametric and external excitation. *J. Appl. Mech*, 57(1), 209–217.

Yoo, H.W., Riegler, R., Brunner, D., Albert, S., Thurner, T., and Schitter, G. (submitted). Vibration influence evaluation of MEMS scanning system for automotive lidar.